Geological context and vents morphology of the ultramafic-hosted Ashadze hydrothermal areas (Mid-Atlantic Ridge 13°N)

Hélène Ondréas, Mathilde Cannat, Yves Fouquet, Alain Normand

Geochemistry Geophysics Geosystems G3

Article
Volume 13, Number 1
6 November 2012
Q0AG14, doi:10.1029/2012GC004433
ISSN: 1525-2027

Published by AGU and the Geochemical Society

Geological context and vents morphology of the ultramafic-hosted Ashadze hydrothermal areas (Mid-Atlantic Ridge 13°N)

Hélène Ondréas
IFREMER, Centre de Brest, Géosciences Marines, BP 70, FR-29280 Plouzané, France (helene.ondreas@ifremer.fr)

Mathilde Cannat
Institut de Physique du Globe de Paris, Sorbonne Paris Cité, Université Paris Diderot, UMR 7154 CNRS, 1 rue Jussieu, FR-75238 Paris CEDEX 05, France

Yves Fouquet and Alain Normand
IFREMER, Centre de Brest, Géosciences Marines, BP 70, FR-29280 Plouzané, France

[1] Recent ROV dives and high-resolution bathymetric data acquired over the Ashadze fields on the Mid-Atlantic Ridge (13°N) allow us to derive constraints on the regional and local geological setting of ultramafic-hosted hydrothermal fields. The active vent fields of Ashadze hydrothermal fields are located in the western axial valley wall, downslope from the termination of a prominent corrugated surface and in a transitional domain with respect to ridge segmentation. The study of the shipboard and ROV bathymetry shows that decameter (100 m by 60 m) to kilometer-scaled rockslides shape the axial valley wall slopes in this region. The Ashadze 1 vent field occurs on a coherent granular landslide rock mass that is elongated in an E-W direction. The Ashadze 1 vent field comprises hundreds of active and inactive sulfide chimneys. The Ashadze 2 vent field is located in a NNE-trending linear depression which separates outcrops of gabbros and serpentinized peridotites. Active black smokers in the Ashadze 2 field are located on ultramafic substratum in a 40-m diameter crater, 5-m deep. This crater recalls similar structures described at some vents of the Logatchev hydrothermal field (Mid-Atlantic Ridge 15°N). We discuss the mode of formation for these craters, as well as that for a breadcrust-like array of radial fissures identified at Ashadze 1. We propose that hydrothermalism at Ashadze can be an explosive phenomena associated with geyser-like explosions. Our study also constrains the geological and geophysical context of the ultramafic-hosted Ashadze hydrothermal system that may use the oceanic detachment fault as a preferred permeability conduit.

Components: 12,600 words, 9 figures.

Keywords: Ashadze; Mid-Atlantic Ridge; hydrothermal activity; hydrothermal explosion crater; ultramafic rocks.

Index Terms: 3017 Marine Geology and Geophysics: Hydrothermal systems (0450, 1034, 3616, 4832, 8135, 8424); 3616 Mineralogy and Petrology: Hydrothermal systems (0450, 1034, 3017, 4832, 8135, 8424); 8135 Tectonophysics: Hydrothermal systems (0450, 1034, 3017, 3616, 4832, 8424).

Received 12 September 2012; **Accepted** 2 October 2012; **Published** 6 November 2012.

Ondréas, H., M. Cannat, Y. Fouquet, and A. Normand (2012), Geological context and vents morphology of the ultramafic-hosted Ashadze hydrothermal areas (Mid-Atlantic Ridge 13°N), *Geochem. Geophys. Geosyst.*, *13*, Q0AG14, doi:10.1029/2012GC004433.

Theme: Oceanic Detachment Faults

1. Introduction

[2] Hydrothermal activity associated with serpentinized ultramafic outcrops was first described at 14°55′N in the eastern rift valley wall of the Mid-Atlantic Ridge [*Rona et al.*, 1987]. Extensive ultramafic-hosted hydrothermal activity also was inferred in this region of the Mid-Atlantic Ridge from water column methane anomalies [*Bougault et al.*, 1990; *Charlou et al.*, 1991, 1998]. Since these early discoveries, other ultramafic-hosted vents have been discovered in the region of the Mid-Atlantic Ridge: Logatchev (14°45′N [*Batuyev et al.*, 1994; *Bogdanov et al.*, 1995; *Krasnov et al.*, 1995; *Charlou et al.*, 2010; *Fouquet et al.*, 2010]), Ashadze (13°N [*Beltenev et al.*, 2002, 2003; *Charlou et al.*, 2010; *Fouquet et al.*, 2010]) and more recently, Semyenov (13°30′N [*Cherkashov et al.*, 2010]) (Figure 1). These discoveries represent a significant addition to the list of ultramafic-hosted vents that have been discovered elsewhere along the Mid-Atlantic Ridge: Rainbow (36°14′N [*German et al.*, 1996; *Fouquet et al.*, 1997; *Charlou et al.*, 2002]), Lost City (30°10′N [*Kelley et al.*, 2001]), Saldanha (36°33′N [*Fouquet et al.*, 1997; *Barriga et al.*, 1998; *Dias and Barriga*, 2006; *Dias et al.*, 2011]), and Nibelungen (8°18′S [*Melchert et al.*, 2008]).

[3] These ultramafic-hosted sites are located on the walls of the axial valley, in areas of extensive outcrops of exhumed mantle-derived rocks with occasional gabbros. These outcrops characterize the less magmatic portions of slow spreading ridges [*Cannat et al.*, 1995], which are frequently, but not exclusively, found near axial discontinuities, at the extremities of ridge segments. Exhumation of mantle-derived material is commonly asymmetric and accommodated on one flank of the ridge by large offset normal faults or detachments [*Karson and Dick*, 1983; *Cannat*, 1993; *Cannat et al.*, 1997; *Tucholke et al.*, 1998; *Smith et al.*, 2006; *Escartín et al.*, 2008]. Some of these detachments display spectacular spreading direction-parallel corrugations [*Cann et al.*, 1997; *Blackman et al.*, 1998; *Escartín et al.*, 2003; *Smith et al.*, 2006; *MacLeod et al.*, 2009].

[4] Ultramafic-hosted hydrothermal fields that vent high temperature, metal-rich fluids (e.g., Rainbow, Logatchev, Niebelungen, Semyenov and Ashadze) are inferred to derive part of their heat, and most of their metals, from interaction with hot and possibly partially molten gabbroic bodies at the ridge axis [*Allen and Seyfried*, 2004]. Low-temperature hydrothermal activity in ultramafic systems also may be driven by the exothermic serpentinization reactions [*Lowell and Rona*, 2002; *German and Lin*, 2004]. Hydrothermal activity in ultramafic seafloor areas is associated with specific fluid compositions, and most notably with the abundance of hydrogen and methane gases [*Charlou et al.*, 1988, 1991; *Rona et al.*, 1992; *Bougault et al.*, 1993; *Charlou et al.*, 1998] which can be generated by serpentinization reactions [*Seyfried and Dibble*, 1980; *Janecky and Seyfried*, 1986; *Wetzel and Shock*, 2000; *Seyfried et al.*, 2007]. At the Rainbow hydrothermal site, for example, fluids have H_2 concentrations of up to 16 mmol/kg and CH_4 concentrations of up to 2.5 mmol/kg [*Charlou et al.*, 2002]. Similar H_2 and CH_4 concentrations have been measured at the Logachev vents [*Douville et al.*, 2002], and recent data on the Ashadze fluids reveal yet higher H_2 concentrations (up to 26 mmol/kg [*Charlou et al.*, 2010]).

[5] Large offset normal faults also called oceanic detachment faults have been proposed to play a major role as permeable channels that allow fluids to reach down to deep gabbroic bodies [*McCaig et al.*, 2007, 2011]. The location of the Semyonov vents [*Cherkashov et al.*, 2010] on a recently exhumed corrugated fault surface at 13°30′N is in good agreement with this interpretation. Sustained hydrothermal activity in this corrugated core complex is attested by one of the largest estimated sulfide deposits in the Atlantic (2700 m by 1600 m), resulting in an estimated resource of 13.95 Mt. The U/Th ages is up to 90 kyrs for the sulfides of Semyonov field [*Cherkashov et al.*, 2010]. Younger maximum ages have been obtained for sulfides from the Logatchev (up to 58 kyrs [*Cherkashov et al.*, 2010]) and Ashadze fields (up to 27 kyrs for Ashadze 2, and 7 kyrs for Ashadze 1 [*Cherkashov et al.*, 2010]). This indicates that the heat supply and the permeability pathways for hydrothermal

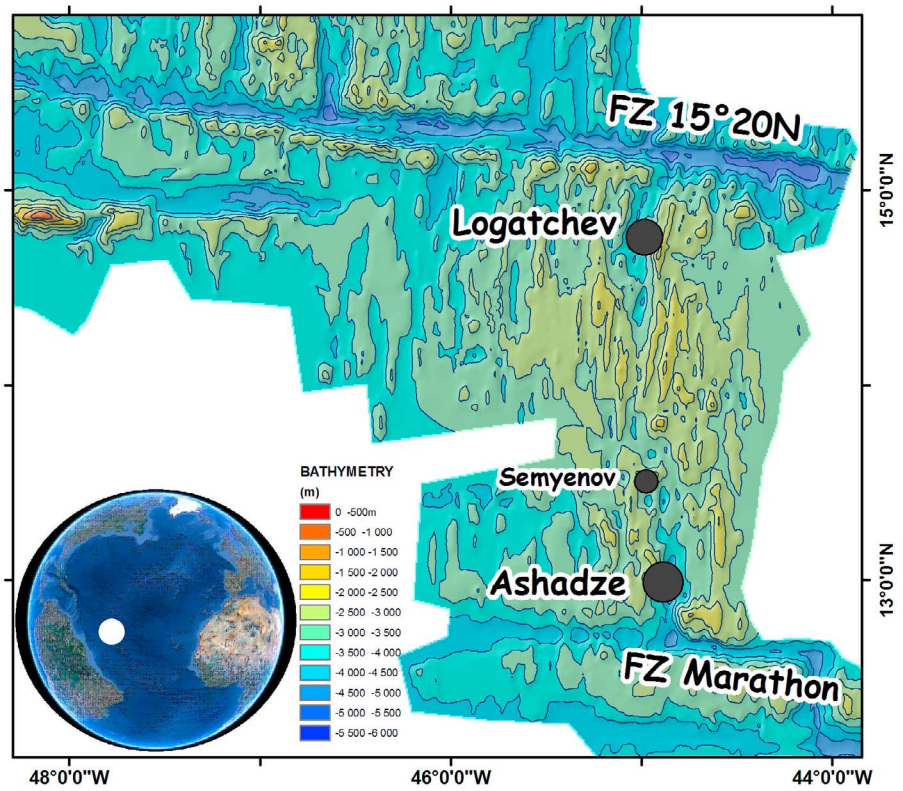

Figure 1. Location of the Ashadze and Logatchev areas on the Mid-Atlantic Ridge south of the 15°20N Fracture Zone.

systems associated with exhumation of mantle-derived material at these sites are maintained, at least episodically, for periods of tens of kyrs. Little is known, however, of the dimensions, geometry and dynamics of these hydrothermal systems. Field studies that document the full variability of settings for these ultramafic-hosted systems are critical to progress in this understanding.

[6] In this paper, we present new geological and high resolution bathymetric data acquired for the two Ashadze vent sites at 12°58′N on the Mid-Atlantic Ridge (Figure 1). Sulfide deposits and water column hydrothermal signals have been discovered at these two sites during Russian cruises [*Beltenev et al.*, 2004]. Black smoker activity was then verified by ROV (Remotely Operated Vehicule) exploration during the Serpentine cruise [*Fouquet et al.*, 2008, 2010; *Charlou et al.*, 2010] with fluid sampling, detailed video observations, further rock sampling, and the acquisition of near-seafloor magnetic maps on the vent fields and a few shipboard magnetic profiles. The high resolution bathymetric maps used in this paper also were acquired during the Serpentine cruise. Ashadze 1 (Figure 2a), at a depth of 4100 m, is the deepest known active vent field along the MAR. Ashadze 2, also active, is located further upslope (Figure 2a), at 3270 m depth. Extinct sulfide chimneys also were observed on highly sedimented seafloor in the axial valley inner trough at 4530 m (Figure 3a). The high resolution (pixel size: 0.5 to 1 m) of the new bathymetric data allows us to derive new constraints on the geological setting of these ultramafic-hosted hydrothermal systems, and to compare it with that of other known ultramafic-hosted hot vents. We specifically address two characteristics of the Ashadze vents: 1- their location with respect to the local ridge segmentation pattern and to the kilometer-scale rockslides that characterize the lower slopes of the rift valley wall in the area (M. Cannat et al., High resolution bathymetry reveals landslide activity shaping the walls of the Mid-Atlantic Ridge axial valley, submitted to *Geochemistry, Geophysics, Geosystems*, 2012); and 2- the detailed morphology of the seafloor in each hydrothermal area and the local distribution of vents. We suggest that these

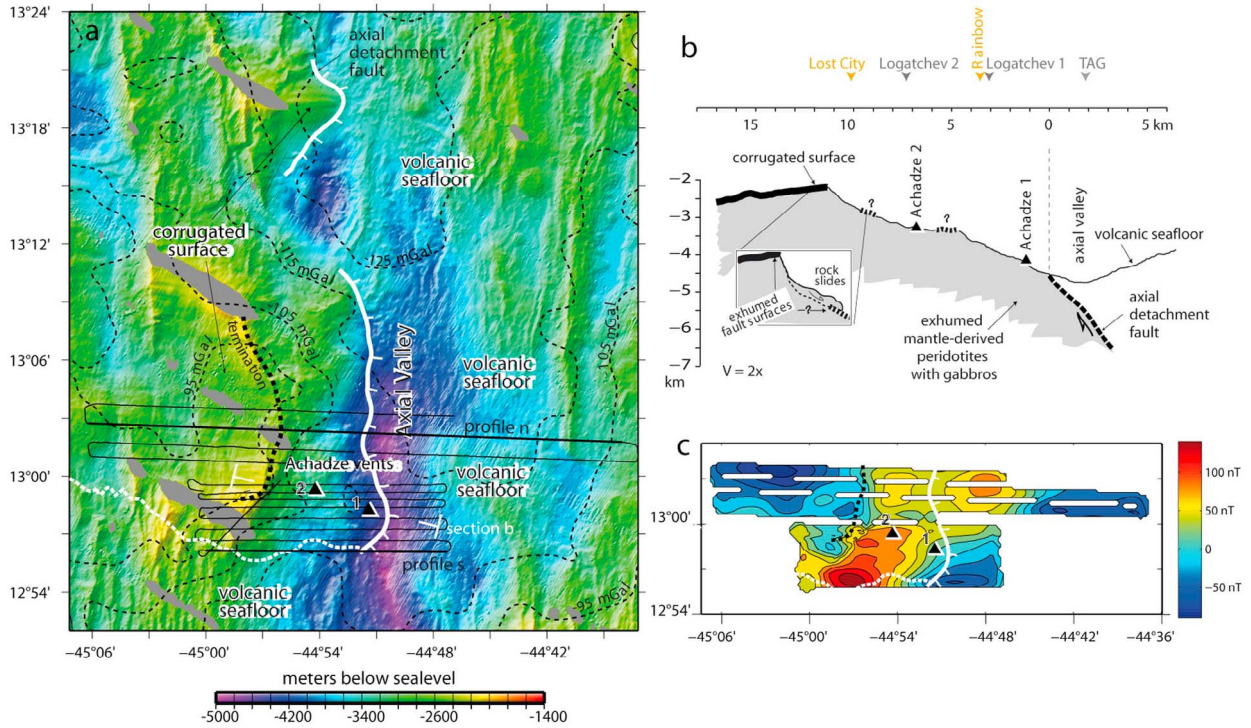

Figure 2. Regional setting of the Ashadze vent fields. (a) Bathymetry [*Smith et al.*, 2006], with selected contours of mantle Bouguer gravity anomaly (computed for a model crust of constant thickness: 6 km, and density: 2700 kg/m^3 [*Smith et al.*, 2008]), and location of the two Ashadze vent fields, of the section shown in Figure 2b, and of the shipboard magnetic profiles used to derive (c) the magnetic anomaly map. 2D models of magnetic anomalies for profiles n and s are shown in Figure 8. (b) Bathymetric section across the Ashadze vent fields with interpretative tectonic sketch showing inferred active detachment fault (bold line, long dashes), exposed corrugated detachment fault surface (bold line), and possible remnants of eroded exposed detachment surfaces (bold line, short dashes) in the western wall of the axial valley at lat. 13°N. The sketch in inset shows that seafloor exposures of ultramafic rocks are interpreted as made either of portions of the exhumed fault surface, or of landslides. The distance scale gives distance to inferred point of emergence of the detachment fault (dashed vertical gray line). For comparison, we also show (in gray) the distance of the ultramafic-hosted Logatchev hydrothermal vents and of the basaltic-hosted TAG vents to the inferred point of emergence of the detachment fault at their respective locations [*Petersen et al.*, 2009; *deMartin et al.*, 2007]. In yellow, we show the distance between other MAR ultramafic-hosted hydrothermal vents (Rainbow [*Fouquet et al.*, 1997] and Lost City [*Kelley et al.*, 2001]) and the deepest point of the axial valley at their respective locations (location of fault emergence not known).

characteristics support that hydrothermal activity at the Ashadze sites is periodically explosive.

2. Methodology and Data

[7] *High resolution bathymetry.* During the Serpentine cruise of R/V Pourquoi Pas?, high-resolution bathymetry and backscatter data were acquired using the "Module de Mesures en Route" (MMR) deployed on ROV Victor 6000 [*Siméoni et al.*, 2007; *Ondréas et al.*, 2009], with a RESON SeaBat 7125 multibeam echo sounder. The system operates at a frequency of 400 kHz, to a maximum altitude (H) of 200 m above seafloor. At an altitude of 100 m, it offers up to 120° swath coverage. It has a horizontal resolution of 5% of H, and a bathymetric accuracy of 0.2% of H. The ROV Victor is navigated with an ultra-short baseline system. Accuracy of this navigation is about 1% of seafloor depth. In the Ashadze 1 area (Figure 1), we conducted surveys at an altitude of 50 m above seafloor, covering about 3 km^2. We also conducted more detailed surveys at an altitude of 20 m over the Ashadze 1 and Ashadze 2 vent fields, covering about 0.3 km^2 in each survey. These high-resolution ROV bathymetry data were processed with the CARAIBES® software (Ifremer), and gridded at 1-m spacing for the data acquired at an altitude of 50 m, and at 0.25-m spacing for the data acquired at an altitude of 20 m.

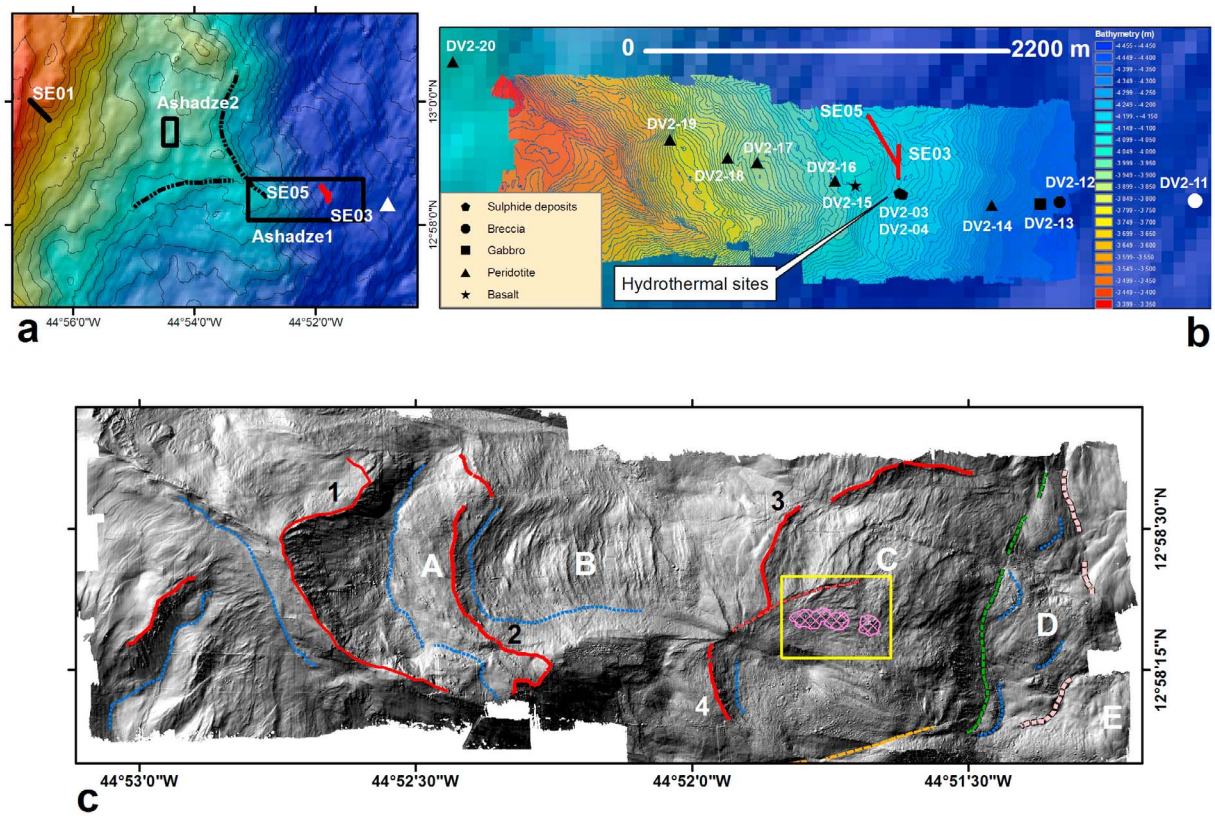

Figure 3. (a) Local setting of the Ashadze vent fields in the MAR western axial valley wall. Dredge tracks (SE) are shown as red and black lines. The horseshoe-shaped scars of two kilometer-scale landslides (see text) are shown as black dashed lines. Black boxes show location of high resolution maps shown in Figures 3b and 3c for the Ashadze 1 area, and in Figure 4 for the Ashadze 2 area. The white triangle shows the position of fossil sulfide chimneys in the axial valley. (b) High resolution bathymetric map of Ashadze 1. Isobaths every 10 m. Symbols show location of dive samples. Red lines are dredge tracks. The location of hydrothermal sites is shown (c) Grey-shaded high resolution bathymetric map of Ashadze 1. Letters and numbers are referred in the text. Red lines mark the edge of the main scarps, and blue dashed lines mark their foot. The yellow box shows location of the shaded relief map in Figure 6 and pink lines limit the hydrothermal area. The dotted orange line is an inferred sub-vertical tectonic lineament (see text). The hatched green line marks the foot of a lineament inferred to be the present-day emergence of the oceanic detachment fault (see text). The pale pink line possibly represents start of the domain not disturbed by landslides. Letters A, B, C, D and E represent the different domain of landslides as described in text. Numbers 1, 2, 3, 4, represent heads of scarps (see text).

[8] *ROV dive observations*. We used the GIS ArcMap-based ADELIE software (Ifremer Data Processing Department) to process and display ROV videos, photographs, and sampling locations.

[9] *Shipboard magnetics*. Short shipboard magnetic profiles were acquired during the Serpentine cruise in periods of ROV maintenance with a SMM2 GEOMAG scalar magnetometer, towed 300 m behind the ship. Eight E-W profiles, including profile s, each with a distance of 0.8 nautical miles cover the Ashadze areas. Two longer profiles, including profile n, cross the axial valley northern (Figure 2a). The data were acquired every 5 s at ship speeds of 4.5 to 11 knots. Raw magnetic data were then averaged over 45 s and filtered for noisy intervals (std >5 nTesla for the 9 averaged measures). Values of the IGRF at corresponding locations were calculated using a script written by Maurice Tivey. The computed anomaly was gridded at 300-m spacing (Figure 2c).

3. Regional Setting of the Ashadze Vents Fields

[10] The active Ashadze vents fields are located 30 km to the north of the Marathon Fracture Zone (Figure 1) in the western wall of the Mid-Atlantic Ridge axial valley (Figures 2a and 2b). The full

spreading rate derived from magnetic anomalies in this region of the MAR is 25 km/myrs [*Fujiwara et al.*, 2003]. The venting areas are found at depths of 4070 to 4100 m for Ashadze 1, and 3250 to 3270 m for Ashadze 2, and at distances of respectively 3.2 km and 7.5 km along a flow line (azimuth ca 95°) from the deepest point of the axial valley (Figure 2b). A single extinct sulfide chimney also was observed (sample DV2–11 massive sulfides, dominantly sphalerite with silica and marcasite; Figure 3b) at a depth of 4530 m during ROV dive 311–02, on the same flow line as Ashadze 1. It should be noted that the Ashadze 3 sulfide deposit reported by *Beltenev et al.* [2005] 1.8 km to the north of the Ashadze 1 vents, was not found again during the 2007 ROV investigation of the lower axial valley wall slopes.

[11] The Ashadze 1 and 2 active vent fields are located downslope from the termination of a prominent corrugated surface that caps the axial valley wall (Figure 2a) [*Smith et al.*, 2006]. The bathymetrically lower Ashadze 1 rests on relatively steep slopes (18° on average), while the upper Ashadze 2 is set on gentler slopes (Figures 2b and 3a). We interpret the hemi-circular scarps along the edge of the Ashadze 2 terrane (dashed lines in Figure 3a) as head scarps for kilometer-scaled rockslides that shape the lower axial valley wall slope in this region. Sampling by dredging and submersible dives during the Serpentine cruise (Figure 3b) complemented earlier sampling by Russian cruises [*Beltenev et al.*, 2003; *Cherkashov et al.*, 2008, 2010], showing that this entire section of the axial valley wall is dominated by ultramafic lithologies, with less common gabbros. One dredge (SE01; Figure 3a) at the termination of the corrugated surface above the hydrothermal fields recovered abundant greenschist facies sheared gabbros and basalts, together with serpentinized and talc-rich ultramafics [*Picazo et al.*, 2012]. While corrugated seafloor has been shown to correspond to exhumed and rotated fault surfaces [*MacLeod et al.*, 2002, 2011; *Escartín et al.*, 2003; *Smith et al.*, 2006], it was not clear from shipboard bathymetry alone if the ultramafic exposures that host the Ashadze vents are also fault rocks, represent deeper levels in the footwall of the fault that would have been exposed by landslides, or are landslide deposits (inset in Figure 2b). Our study of the higher resolution near-bottom bathymetry allows us to address this question at least in the case of the Ashadze 1 vent field.

[12] The corrugated surface above the vent fields extends about 20 km along axis. To the south, it ends into a domain of regularly spaced abyssal hills that is interpreted as volcanic seafloor [*Smith et al.*, 2008]. This volcanic seafloor domain forms a spreading-parallel corridor that extends from the Marathon FZ in the south to about 6 km from the Ashadze vent fields to the north (Figure 2a). Shipboard gravity data reported by *Smith et al.* [2008] show that this volcanic domain is characterized by more negative mantle Bouguer gravity anomalies (MBA) than the exhumed ultramafic domain to the north. The MBA low (MBA < −115 mGal in Figure 2a) in the volcanic seafloor corridor is actually offset to the west of the axial valley, while conjugate seafloor in the eastern ridge flank has less negative MBA, and a higher elevation. North of the vent fields, by contrast, the MBA low is offset some 10 km to the east of the deepest point of the axial valley, in an area of volcanic seafloor morphologies (Figure 2a). This unusual axial gravity anomaly pattern is echoed by the magnetic anomalies recorded over the Ashadze area during the Serpentine cruise (Figure 2c). Positive magnetic anomalies characterize the axial valley to the north of the Ashadze vent fields, with a lesser magnetic high on the western axial valley wall. By contrast, the axial valley south of the vent fields coincides with a distinct magnetic low, and the magnetic high is offset to the west (Figure 2c). The axial valley wall at the latitude of the vent fields corresponds to a broad magnetic high.

4. Local Setting of the Ashadze Hydrothermal Vents

4.1. Local Setting of the Ashadze 1 Vents

[13] We acquired two sets of microbathymetric data over the Ashadze 1 area. One set, acquired at an altitude of 50 m, was gridded at a spacing of 1 m and covers the axial valley wall slopes above and below the vents (Figure 3). The other, acquired at an altitude of 20 m, is centered on the hydrothermal field and gridded at a spacing of 25 cm. The 50-m high survey data (Figure 3) show from west to east a succession of east-facing horseshoe-shaped scarps that we interpret as landslide head scarps. A detailed analysis of seafloor morphologies in this high-resolution map is given in Cannat et al. (submitted manuscript, 2012). Here, we outline the principal landslides units and focus on their relation with the Ashadze 1 vent field.

[14] The first scarp to the west in the mapped area (scarp 1 in Figure 3c) develops at the junction between the two larger head scarps shown in

Figure 2a. Scarp 1 has a diameter of about 700 m and accommodates a 200 m drop of the downslope terrane (A in Figure 3c). Serpentinized peridotites (ROV sample DV2–19; Figure 3b) were sampled in this first scarp. Landslide terrane A is cut by 2 linked horseshoe scars that accommodate an additional 100 m drop (scarp 2 in Figure 3c). The domain below scarp 2 (labeled B in Figure 3c) shows a series of 1-to 5-m-high cuspate ENE-facing scarps interpreted as multiple slope-failure features. In ROV videos, this area corresponds to a succession of small sedimented scarps with occasional talus of serpentinized peridotite (ROV samples DV2–18, DV2–17, DV2–16) and basalt (DV2–15). At a depth of about 4030 m, landslide terrane B is cut by scarp 3 (25 m-high). Seafloor below scarp 3 (landslide terrane C) has a fabric of NNE-and NE-trending joints that suggests that it is a more coherent rock mass than the pervasively fractured material of domain B. To the south, scarp 3 is cut by yet another landslide scar (scarp 4 in Figure 3c). The Ashadze 1 vents are located at the junction of these scarps, and aligned in an E-W trend. The vents are set in talus of serpentinized peridotite, a few meters to the south of the jointed outcrops which are part of coherent landslide rock mass C (Figure 3c). ROV dives imaged sedimented talus deposits next to the vents. ROV (DV2–03 and DV2–04) and dredge samples (SE03 and SE05; Figure 3b) are serpentinized peridotites with occasional metagabbroic veins and local talc replacement [*Picazo et al.*, 2012].

[15] Below the vents, slopes become steeper (>30°) over the full width of the mapped area. These steeper slopes (green lineaments in Figure 3c) expose serpentinized peridotites (sample DV2–14) and are affected by recent erosion in the form of decameter-sized excavations and gullies. Two observations lead us to infer a tectonic origin for this steep slope: it is linear and not convex-downward typical of landslide head scarps and there is a clear slope break between this steep slope and the more gently sloping debris lobes below (domain D in Figure 3c). Based on its orientation and recent erosion, we interpret this steep slope as marking the present-day point of emergence of the active oceanic detachment fault. The Ashadze 1 vents are located only 600 m to the west of this inferred fault emergence. ROV dives sampled a tectonic ultramafic breccia (DV2–12), and a metagabbro (DV2–13) in the debris lobes of domain D. The distance between the master landslide head scarp 1 above domain A and the debris lobes of domain D is 2.6 km (Figure 3c), and the cumulated vertical displacement along this master slide is >300 m (cumulated height of scarps 1 and 2).

[16] Another feature of the map that is probably tectonic in origin is an ENE-trending lineament in the southeast corner of our mapped area (Figure 3c). It cuts across slope which suggests that it corresponds to a sub-vertical event, and it is marked either by a 2-to 5-m-wide depression, or by a meter-high north-facing scarp. It also appears to cut through the gullies of the steep slopes domain. We interpret this lineament as a recent ENE-trending strike slip fault. The Ashadze 1 vents are located only 450 m to the north of this inferred strike slip fault.

4.2. Local Setting of the Ashadze 2 Vents

[17] The Ashadze 2 microbathymetric data was acquired at an altitude of 20 m, and gridded at a spacing of 25 cm. To the southeast, this map shows steeper slopes associated with a kilometer-scaled horseshoe landslide scar (Figure 4a). On the central part of the area three slightly offset linear NNE-trending narrow depressions (50 m-wide or less; Figure 4b) extending to the northern limit of the map take place. To the east of these depressions are two main hills, 200 to 300 m across. The southern one was explored by a ROV dive and is made of massive gabbros (Figure 4d). To the west of the linear depressions we mapped a series of east-facing, meter-high scarps, and a ridge made of aligned knobs, a few decametres across (Figure 4a). This ridge is about 300–400 m long and 10-to 30-m-high and bears several fossil hydrothermal chimneys 1-to-2-m-high (Figure 4c). The active Ashadze 2 black smokers (Figure 4e) vent is in a crater 40 m in diameter and about 5 m deep (Figure 4b), which is located near the southern end of this ridge, in one of the NNE-trending depressions. We sampled sulfides, serpentinite and serpentinite breccia next to this crater (Figures 4 and 5). Diffuse fluid emissions also were observed on the ridge 40 m to the west of the crater (Figure 4f). Just north of the crater, the eastern wall of the NNE-trending depression is an 80 m-high outcrop of massive gabbros, with joints and a decameter-sized striated fault plane, trending NE with a steep western dip and nearly E-W striations (Figure 4d).

[18] The knobby ridge is not present to the south of the venting crater (Figure 4a). At this place the NNE-trending depression is bound by east-facing scarps and ends about 50 m from the steep and eroded landslide scar (Figures 4a and 4b). However, near the southern edge of our mapped area

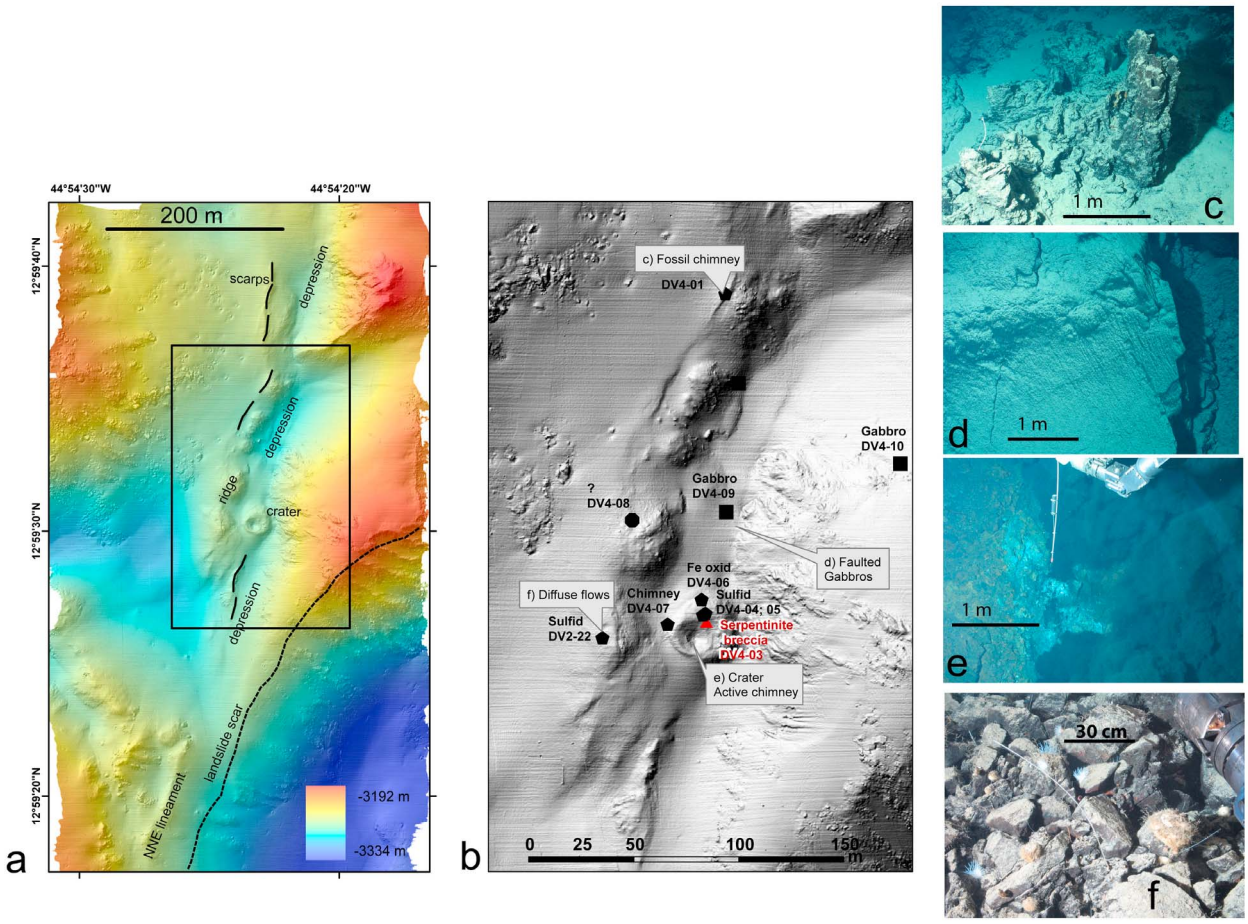

Figure 4. (a) High resolution bathymetry of the Ashadze 2 area showing the location of the hydrothermal crater in a NNE-trending lineament comprised of small scarps and elongated depressions. Dotted black line shows the edge of a scarp interpreted as the head scarp of a large landslide (see text). Black box shows location of detailed map shown in Figure 4b. (b) Shaded bathymetry next to the Ashadze 2 hydrothermal crater with location of seafloor pictures (Figures 4c–4f). Symbols show location of dive samples. Sample sites also shown; symbols are the same as in legend in Figure 3b. (c) Fossil hydrothermal chimney; (d) massive gabbros cut by fault plane bearing E-W striations; (e) black smoker in the hydrothermal crater; (f) diffuse venting in sulfide and serpentinized peridotite debris pile.

(Figure 4a), the high-resolution bathymetry shows a ridge-like NNE-trending lineament and a small rounded hill that looks like the knobs on the ridge further north. It is thus possible that the NNE-trending lineament that hosts the Ashadze 2 vent system extends over the entire mapped area.

5. Morphology of the Hydrothermal Vents and Mineralogy of the Hydrothermal Deposits

[19] In this section, we use high-resolution bathymetry and ROV dive observations to present the distribution and morphology of active and inactive vents at Ashadze 1 and 2. We also present an outline of the mineralogy of hydrothermal deposits from *Fouquet et al.* [2010], and note the maximum fluid temperatures (some reported in *Charlou et al.* [2010]) for the active vents.

5.1. Ashadze 1

[20] High-resolution bathymetry acquired at an altitude of 20 m (25 cm grid) reveals the detailed structure of the hydrothermal field (Figure 6, center). The active hydrothermal area at Azhadze1 extends from 4065 to 4120 m, over a 180 m-long, 60 m-wide area elongated in a general W-E direction. It is the deepest active black smoker area discovered on the MAR to this date. The high resolution map shows that the hydrothermal field can be divided into three parts (Figure 6, center): a granular area with active chimneys to the west;

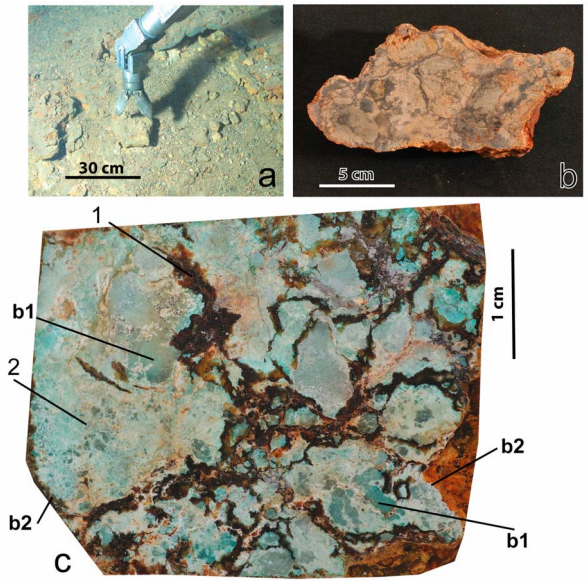

Figure 5. (a) ROV sampling of the inner part of the Ashadze 2 crater (DV04–03, see Figure 4 for position); (b) Photo of the sample showing the brecciated structure of the ultramafic rock; (c) polished section showing multigenerational breccia with late copper-sulfide veining: 1 – dark veins are primary made of chalcopyrite and isocubanite, 2 – multigenerational breccia (serpentinite and talc) where both b1 and b2 breccia generations are shown.

a zone with a radial array of fissures, recalling the crust of a bread loaf (breadcrust-type structure) at the eastern end of the granular area (details in Figure 7e); and a circular area about 15 m in diameter with numerous fossil chimneys, about two hundred meters to the east, at a depth of 4145 m. The inactive chimneys there are 1 to 3 m in high.

[21] The granular area forms a 60-m-by-100-m mound, about 6 m higher than the surrounding seafloor (center of Figure 6). ROV observations reveal that the seafloor on this mound is composed of hundreds of sulfide chimneys, most of which are less than 3 m-high (Figure 6c), and highly altered serpentinite. The large number of chimneys indicates that the discharge of hydrothermal fluids is distributed over a relatively large area. Similarly distributed venting has been observed at other ultramafic hosted deposits such as Rainbow [*Fouquet et al.*, 1997] and Logatchev [*Petersen et al.*, 2009]. The chimneys are made mostly of isocubanite ($CuFe_2S_3$) and chalcopyrite in the central part and sphalerite and wurtzite in the outer part. Pyrite and pyrrhotite are common but not abundant in these tightly spaced chimneys. This mineralogy indicates that most chimneys were formed by high temperature (>300°C) fluids. Four groups of active chimneys, named SE1, SE2, SE3, and SE5 (Figures 6a, 6b, 6c, and 6d) have been identified. SE1 (4087 m;

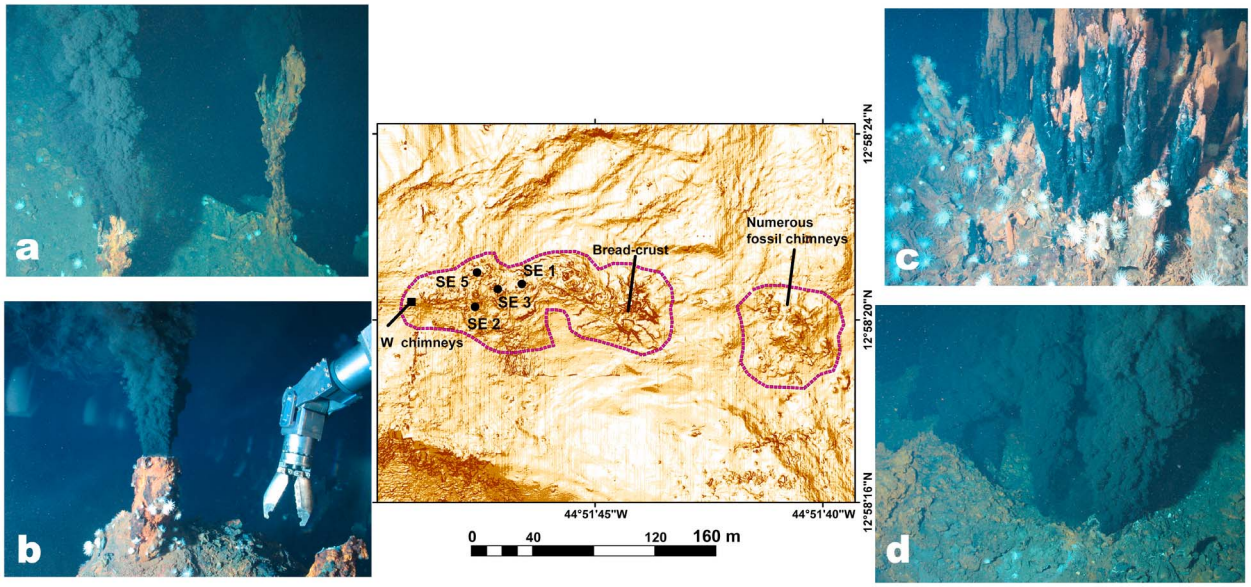

Figure 6. In the center, shaded high resolution bathymetry of the Ashadze 1 hydrothermal area with location of the main vents (seafloor photographs (Figures 6a, 6b, 6c and 6d) are located with respect to these vents), chimneys in the west part (noted W chimneys) and fossil chimneys (see text). Purple lines delimit the hydrothermal area. Seafloor photographs: (a) two black smoking chimneys (SE5); (b) the SE2 black smoker; (c) the "Anemones garden" site (SE1); (d) the SE3 black smokers.

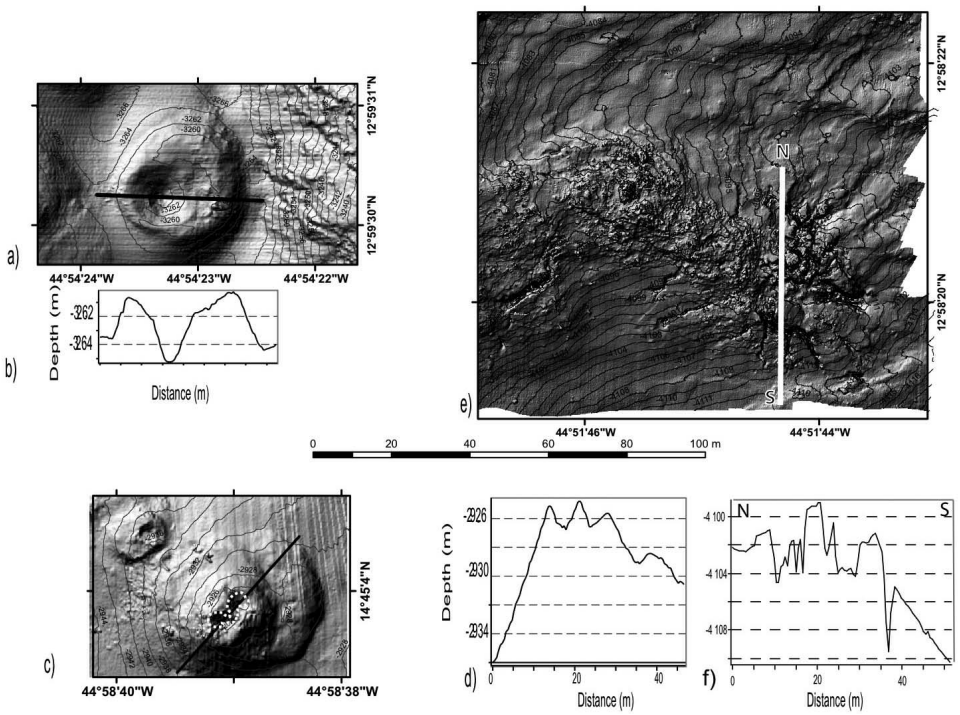

Figure 7. Seafloor morphologies that may be due to explosive hydrothermal activity. Maps and sections are shown at the same scale, sections have a vertical exaggeration of 3.5. (a and b) Map and section of the hydrothermal crater at Ashadze 2 (location in Figure 4); (c and d) map and section of the Anne-Louise hydrothermal crater at Logatchev; dotted white line represents the limit of the crater; (e) map of breadcrust-like seafloor structure at Ashadze 1 (location in Figure 6); (f) section across breadcrust-structure.

Figure 6c) is 15 m by 25 m and has more than one hundred chimneys. Some inactive chimneys are 3-m-high and a few tens of centimeters in diameter. The active chimneys are 50 cm high most and 10 cm in diameter; vent fluids have a maximum measured temperature of 159°C. SE2 (4085 m; Figure 6b) is an isolated chimney, 20 cm in diameter and 2-m-high (before being broken for fluids sampling) that tops a 1-m-high, 2-m diameter mound of hydrothermal deposits. This chimney expels fluids at a measured temperature of 352°C. SE3 (4090 m; Figure 6d) has ten very active black smokers, some of which vent directly from the seafloor. The maximum temperature measured there is 372°C. Finally SE5 (4080 m; Figure 6a) comprises two active chimneys (1 m and 50 cm high), with fluids measured at a temperature of 347°C. To the west of this active granular area, a few isolated thin chimneys, up to 2 m high but only 20 cm in diameter (W in Figure 6, center) vent low-temperature (100°C) fluids. To the east of the active granular area, the "breadcrust" structure is 70 m by 70 m with fissures radially distributed from a central point at about 4104 m (Figures 7e and 7f). Taking account the local slope, the cross-section of this area (Figure 7f) shows a very rough and fissured seafloor, forming a dome 40 m in diameter, and some 6 m-higher than the surrounding seafloor. Fissures are 1-to 2-m-deep, and 1 to 4 m wide. No hydrothermal vents have been seen during the dives in this fissured area but also on the backscatter data. The fossil site (Figure 3a), at a depth of 4526 m in the axial valley, is basalt hosted. It comprises only one fossil 1 m high chimney made of massive sulfides, dominantly sphalerite with silica and marcasite.

5.2. Ashadze 2

[22] Active black smokers at Ashadze 2 vent from the middle of a hydrothermal crater at a depth of 3260 m (Figures 4 and 7a). The crater is about 5 m-deep and 40 m in diameter (Figures 7a and 7b). It is comparable to the Anne-Louise crater at the Logatchev hydrothermal field [*Petersen et al.*, 2009] (Figures 7c and 7d). Fluids vent from the bottom of the crater, out of numerous small chimneys (Figure 4e). A maximum temperature of 296°C was measured for these fluids but measurements were difficult because the ROV could not be positioned adequately in the bottom of the crater. The true temperature is therefore probably higher. The crater's ring is asymmetrical. Detailed sampling

shows that the ring crater is composed of ultramafic multigenerational breccia (Figures 4 and 5). Breccia elements are made of serpentinite and talc. Sulfide veins in the breccia are primarily composed of isocubanite and chalcopyrite. The crater is also composed of aragonite occurring sometimes as chimneys. This aragonite shows numerous atacamite ($Cu_2Cl(OH)_3$) patches. A fossil 2-m high chimney was seen on the west side on the top of the crater's ring. The central part of the crater is occupied by sulfidic copper-rich chimneys, up to 20 cm-high. Fragments of sulfide chimneys were also observed on the northern and eastern external sides of the ring. Very discrete active diffuse discharge was observed outside of the crater, and shimmering waters occur about 40 m to the west (Figure 4f). Extinct chimneys made of Fe-oxides, porous sphalerite, and aragonite also were sampled about 170 m to the north of the crater. The extinct chimney shown in Figure 4c is 1 m 50 high and 50 cm in diameter at the top, 1 m diameter at the base.

6. Discussion

6.1. Geological Setting of the Ashadze Vents: Links With Axial Discontinuity, Detachment Fault and Rockslides

[23] *Axial discontinuity*. The ridge section that hosts the Ashadze fields is orthogonal to spreading. It is characterized by a deep axial valley that shows no offset all the way to the Marathon FZ 30 km to the south (Figures 1 and 2a). Yet, seafloor morphology, gravity, and magnetic data indicate that the Ashadze vents are located in a transitional domain with respect to axial segmentation. This domain is comparable to the ridge further to the north in that the western axial valley wall exposes serpentinized peridotites and gabbros and has a more pronounced bathymetry and a less negative gravity signature than the eastern axial valley wall (Figure 2). Less than 10 km to the south of the Ashadze vents, however, the seafloor in the western axial valley wall displays typical volcanic morphologies. The available magnetic data is scarce, but indicates that a pronounced positive magnetic anomaly is centered below the western axial valley wall in this volcanic domain (Figure 2c). 2D models made with the ModMAG software [*Mendel et al.*, 2005] for magnetic profiles south of the vents (located in Figure 2a, see also Figure 8) are consistent with an offset of the magnetic axis to the west of the deepest point of the axial valley, by about 20 km (Figure 8). If this interpretation is correct, and given the volcanic nature of the seafloor in this southern domain, the offset of the magnetic axis is most likely to result from an offset of the most recent volcanic activity to the west of the axial valley trough. This would be consistent with the observation of a local MBA minimum [*Smith et al.*, 2008] in this volcanic domain, which also is offset to the west relative to the deepest part of the axial valley (Figure 2a). For magnetic profile n, located to the north of the vents, 2D modeling suggest either an 80% asymmetry of recent spreading with faster rates to the west, or a 10 km recent offset of the magnetic axis to the west (Figure 8). Our magnetic data set is too scarce to discriminate between these two hypotheses.

[24] *Detachment fault*. The Ashadze hydrothermal vent fields belong to the growing family of ultramafic-hosted fields discovered at slow-spreading ridges. Similar to other well documented members of this family, Ashadze 1 and 2 are set in the footwall of the axial valley bounding normal fault that brought the ultramafic host material to the outcrop. With a full spreading rate of 25 km/myrs [*Fujiwara et al.*, 2003], and assuming that oceanic detachment faults take up between 50% and as much as 80% [*Searle et al.*, 2003; *Baines et al.*, 2008; *Dick et al.*, 2008; *Grimes et al.*, 2008; *MacLeod et al.*, 2009] of the whole plate separation, the location of Ashadze 2 (Figure 2b) corresponds to seafloor ages of 350 to 560 kyrs. For Ashadze 1, crustal ages determined with the same method range between 90 and 144 kyrs. Lithologies are dominantly ultramafic next to Ashadze 1. Ashadze 2, however, is set on ultramafics next to outcrops of massive gabbros. It is possible that this lithological contrast enhanced crushing of the softer serpentinized ultramafics next to the harder gabbros during the last stages of exhumation of these deeply derived rocks in the footwall of the oceanic detachment fault.

[25] Some MAR ultramafic-hosted fields (Rainbow and Lost City) are located at or very near axial discontinuities with significant offsets. The Logatchev vent field, similar to the Ashadze vents studied here, is set in more continuous ridge sections, yet displays characteristics that have been interpreted in terms of proximity to small or zero offset axial discontinuities [*Cannat et al.*, 2007; *Petersen et al.*, 2009]. In Figure 2b, we plot these other well documented ultramafic-hosted vent fields (Rainbow, Logatchev, Lost City) as a function of their distance to the foot of the axial valley wall, which we infer represents the most distal possible location for the point of emergence of the oceanic detachment fault. This exercise shows that these sites are spread over a

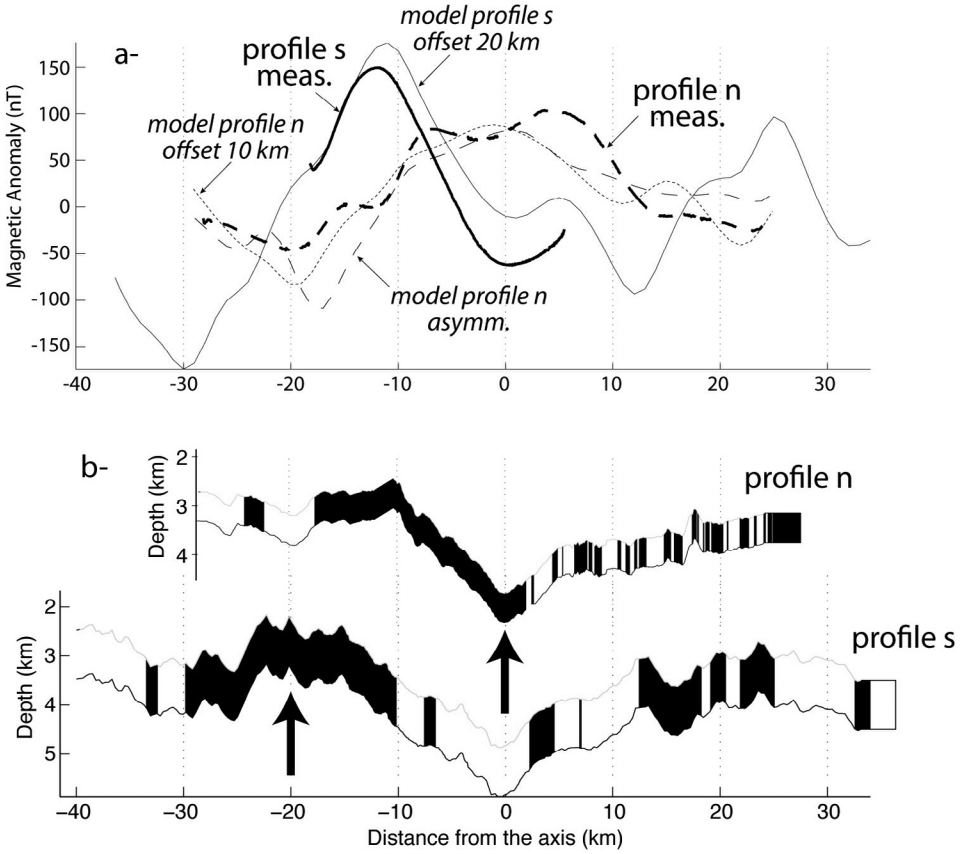

Figure 8. (a) 2D models of magnetic anomalies generated with the ModMAG software [*Mendel et al.*, 2005] for profiles s and n (located in Figure 2a) and for the distribution of magnetic blocks shown in Figure 8b. Measured anomalies are shown as thick lines and modeled anomalies are shown as thin lines (continuous for profile s and dashed for profile n). (b) Distribution of magnetic blocks for symmetric spreading at a constant rate of 25 km/Myr, with a N95 spreading direction. Best fit with measured profile s is obtained for a 20-km offset of the magnetic axis (thick arrow) to the west of the deepest point of the axial valley and a 1-km-thick magnetic layer (distribution of magnetic blocks shown in Figure 8b). Reasonable fits with measured profile n (thick black line) are obtained with a 0.6 km-thick magnetic layer and either 80% asymmetry of spreading (long dashes); distribution of magnetic blocks shown in Figure 8b, or a 10-km offset of the magnetic axis to the west (distribution of magnetic blocks not shown). Magnetization used for the two profiles is 8 A/m for the axial anomaly, and 5 A/m off-axis.

maximum of 11 km (Lost City) from the fault emergence. Ashadze 1, Logatchev 1 and Rainbow lie within 5 km, while Ashadze 2, Logatchev 2 and Lost City lie between 6 and 11 km into the exhumed domain. This last distance is indeed substantial and has led *Kelley et al.* [2001] to use the term «off-axis» for the Lost City vent field. We would not, however, use this term for Ashadze 2. This vent field, although distant from Ashadze 1 by 5.5 km (Figure 2b), is set in the same geological context. Furthermore, fluid chemistry data have led *Charlou et al.* [2010] to propose that Ashadze 1 and 2 are linked to a single hydrothermal circulation system. Fluids at both sites have similar CH_4 contents (1.2 mmol kg^{-1} for Ashadze 1 and 0.8 mmol kg^{-1} for Ashadze 2) and H_2 contents (19 mmol kg^{-1} for Ashadze 1 and 26 mmol kg^{-1} for Ashadze 2 [*Charlou et al.*, 2010]). They differ in salinity (high salinity at Ashadze 1, low salinity at Ashadze 2), which suggests that they vent the complementary components of a phase-separated hydrothermal system [*Charlou et al.*, 2010].

[26] The conceptual sketch in Figure 9 summarizes our preferred hypothesis for the regional geological setting of the Ashadze vents. It involves the inferred 20-km-westward offset of the volcanic axis in the volcanic domain south of the vents. It also assumes a single overall hydrothermal system, which uses the main oceanic detachment fault (as proposed by *McCaig et al.* [2007]) and the fractured footwall next to it, as permeable channels. In our conceptual sketch, fluids are shown to mine heat from melt or mush zones associated to the

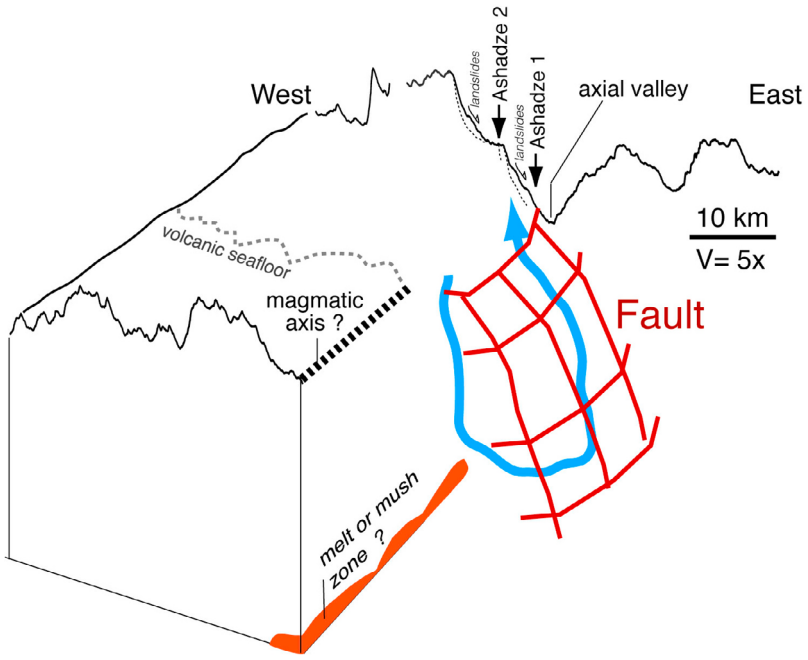

Figure 9. Conceptual sketch of proposed geological settings for the Ashadze vents. The sketch is viewed from the southeast and positioned across the limit drawn in Figure 2a between volcanic and corrugated and/or ultramafic seafloor. In this sketch the same hydrothermal cell system feeds the Ashadze 1 and 2 vents. It uses the east-dipping oceanic detachment fault as a preferred lower permeability conduit and mines heat from magma or hot gabbros emplaced at depth below the volcanic seafloor to the south. Landslides and fissures related to slope failure affect the permeability in the upper few hundred meters below seafloor. The oceanic detachment fault is drawn as a spoon-shaped concave upward structure by analogy with model proposed at TAG [*deMartin et al.*, 2007]. The present-day volcanic axis in the southern volcanic seafloor area is tentatively offset by 20 km to the west of the deepest point of the axial valley, based on available magnetic data (Figure 8).

southern offset volcanic axis. This sketch provides a broad interpretative frame, which should be tested with more detailed geological and geophysical investigations of the Ashadze area. It does not address the question of the actual locations of Ashadze 1 and 2 up the axial valley wall, 0.6 to 6.1 km away from the fault emergence. As mentioned before, this distribution in the detachment footwall is common for ultramafic-hosted vents (see Figure 2 and references therein). It is clearly evidence that hydrothermal flow is not restricted to the main fault, but occurs also in the footwall, at least in the superficial levels.

[27] *Rockslides*. The vents at Ashadze 1 are aligned roughly EW, on the steep slopes associated with a horseshoe-shaped rockslide scar (Figure 3c). This rockslide is the deepest of a series of imbricated slope-failure features, which can be followed downslope from the edge of the Ashadze 2 gently sloping terrane (Figure 3a). Based on the height of the successive head scarps (25 to 200 m; Figure 3c), we infer that the cumulated amount of downslope displacement is of the order of a few hundred meters. We therefore envision that the upper few hundred meters of the ultramafic footwall near Ashadze 1 are cut by imbricated slope failure surfaces. Our interpretation, supported by detailed examination of these slope failure features in Cannat et al. (submitted manuscript, 2012), is that these rockslides are not associated with pervasive disruption of the sliding rock masses. Instead, each imbricated rockslide appears to behave as a relatively coherent rock mass, cut by gravitationally induced extensional fractures and fissures (Figure 3c). The slope-failure surfaces and the associated extensional fractures and fissures could provide high permeability pathways for hot hydrothermal fluids ascending into the ultramafic footwall [*McCaig et al.*, 2007].

[28] The association to slope-failure-related structures is not as obvious as Ashadze 2, but this field is located less than 200 m from the edge of an east-facing scarp that is probably also a large landslide scar (Figure 4). In addition, the NNE-trending depressions that host the Ashadze 2 crater have the right orientation to accommodate gravitationally

induced extension (Figure 4). In the vicinity of the Ashadze 2 vent site, this lineament separates hilly gabbro outcrops to the east from a flatter terrain made of serpentinized peridotite to the west. It is well oriented with respect to the geometry of spreading and may thus be of tectonic origin. It is, however, also perpendicular to the overall direction of maximum slope in the area (Figure 3a). Whether it is tectonic in origin or not, this lineament is therefore well oriented to be reactivated as an incipient slope-failure structure due to the gravitational forces acting on the axial valley wall. The Logatchev vents also have been described as set on an ultramafic rockslide [*Petersen et al.*, 2009], and in the Lost City area, vents are located near the edge of prominent concave-downward cliffs that face the Atlantis transform trough [*Karson et al.*, 2006] and likely represent rockslide scars. The association with gravitational slope-failure features may therefore be a common characteristic of MAR ultramafic-hosted vents.

6.2. Smoking Craters: Result of Explosive Hydrothermal Venting?

[29] The hydrothermal crater at Ashadze 2 (Figure 7a) vents high-temperature fluids, which we would expect to rapidly build anhydrite, then sulfide chimneys. However, the chimneys in the crater are very small, broken fragments of chimneys are observed on the sides of the ring of the crater. High-temperature fluids and smoking craters also are observed at Logatchev, where they have been first described by *Bogdanov et al.* [1997] and *Gebruk et al.* [1997]. *Petersen et al.* [2009] further described the hydrothermal craters (Quest, Site B, Irina1, Candelabre and Anne-Louise) of the Logatchev 1 area. Some craters show black smokers activity or fossil chimneys on the rim (Quest, Site B and Irina1). *Petersen et al.* [2009] also described red serpentinites breccia on the Irina 1 crater rim. We focus our comparison on the Anne-Louise crater, the biggest crater at Logatchev and the most similar in size to the Ashadze 2 crater. The outer rim of the main Anne Louise crater is about 15 m in diameter. It contains 2 depressions, 7–8 m in diameter and 2–3 m deep, separated by a central ridge (Figures 7c and 7d). In the southwestern depression *Gebruk et al.* [1997] described one small chimney, but a survey performed in 2007 [*Petersen et al.*, 2009] documented only black smoke emanating from holes in the ground in both depressions. The difference between these observations indicates that chimneys in this depression got destroyed between the two surveys. *Petersen et al.* [2009] also described small chimneys, up to 30 cm in height, in the exterior wall of the Anne Louise crater.

[30] During the Serpentine cruise which took place in 2007, we also observed smoking holes in the ground, and small chimneys in the rim of the crater. The crater rim of Anne-Louise is made of dominantly decimeter-sized blocks which have greenish and reddish colors suggesting altered serpentinites, and oxidised sulfides or a combination of both. Collected samples show highly altered serpentinite composed of talc, antigorite, chrysotite and goethite.

[31] An explosive venting hypothesis was proposed by *Petersen et al.* [2009] to explain the craters at Logatchev, together with two other possible mechanisms. One of these involved dissolution of anhydrite leading to caving of the material in the craters, and the other involved washing out of a fine-grained serpentine mud entrained by the venting fluids. These mechanisms are, however, unlikely to have formed the Ashadze 2 crater: its rim is made at least partly of breccia and the morphology of the crater is too regular to be the result of dissolution. Furthermore, collapse due to anhydrite dissolution is not possible when venting is still occurring at temperature well above 160°C (anhydrite stability as shown for the TAG mound [*Tivey et al.*, 1995]). The observation of active venting from holes in the ground or small chimneys in the center and in the rims of the craters at both Ashadze 2 and Logatchev suggests that anhydrite is stable and probably precipitates in the subsurface.

[32] At Logatchev, the craters were stable and active over at least the past 10 years (since the first exploration of this field during the Microsmoke cruise in 1997). Due to the intense high temperature activity and without any dramatic event destroying the chimney we should expect to observe large sulfidic spires in the center of these craters. The very small size or the absence of chimneys in the smoking craters thus suggests a recurring process destroying the growing chimneys. This leads us to favor an explosive venting hypothesis for the formation of the Ashadze 2 and Logatchev crater. At Ashadze 2, the occurrence of multigenerational serpentinite breccia constituting the ring of the crater (Figure 5) can be explained by multiphase hydraulic fracturation both destroying the chimneys and maintaining the crater structure. The occurrence of chalcopyrite veins in this type of breccia clearly indicated interaction between breccia and high temperature fluids (>300°C). Talc may also

have been produced during this process by hydrothermal alteration of the ultramafic clasts.

[33] The breadcrust structure at Ashadze 1 has not been reported at other MAR hydrothermal field locations and is more enigmatic. Radial cracks extending over a diameter of about 40 m rim a central area that is about 10 m in diameter, and surrounded by hemi-circular fissures (Figures 7e and 7f). There are no chimneys, active or dead next to this enigmatic seafloor structure. This breadcrust-structure, over a diameter comparable to that of the Ashadze 2 crater (see bathymetry and cross-section in Figure 7), shows a moderate inflation. It could have formed due to very shallow serpentinization of the ultramafic basement that would have induced swelling and have lifted the upper few meters of outcropping serpentinized material over a diameter similar to that of the craters. Another interpretation, which we find more consistent with the presence of the craters, is based on an analogy with the hydrothermal domes observed in terrestrial hydrothermal environments [*Johnson et al.*, 2003; *Morgan et al.*, 2009]. In Yellowstone Lake and on its shores, such domes have diameters of a few meters to >100 m [*Morgan et al.*, 2009]. The formation on top of these domes is locally silicified, and self-sealing processes are interpreted to play an important role in the development of these hydrothermal structure: *Morgan et al.* [2009] explain them by inflation of an overlying impermeable silica cap by rising hydrothermal gas-rich fluids. Domal features may then be precursors to development of hydrothermal explosions craters.

[34] Hydrothermal explosions, or eruptions, at the origin of craters have been reported on land [*Muffler et al.*, 1971; *Browne and Lawless*, 2001; *Morgan et al.*, 2003, 2009] and in lakes (hydrothermal explosion craters of Yellowstone Lake [*Wold et al.*, 1977; *Morgan et al.*, 2002, 2006, 2009]). These craters are a few meters to >2 km wide, many are composit (Mary Bay, Elliott's craters). In Yellowstone Park, *Morgan et al.* [2006] described "an abrupt drop in pressure that initiates steam-flashing and is instantly transmitted through interconnected fractures, resulting in a series of multiple large-scale explosions and the excavation of an explosion crater." According to *Browne and Lawless* [2001], the mechanism causing hydrothermal explosions is comparable to that of a geyser, in that it involves volume change due to the flashing of boiling water converted to steam that develops far greater energy. The steam phase is able to break, lift and eject fragments of the host rock. *Browne and Lawless* [2001] and *Morgan et al.* [2009] also favor a model in which the explosion proceeds downward after the initial steam flash, as the fluid flashing front descends ahead of the brecciation into the host rock [*McKibbin and Absar*, 1989]. Downward propagation of this boiling front proceeds as long as it generates enough steam to lift the overlying rocks. *Browne and Lawless* [2001] also point out that most of the ejected material falls back into the crater, the depth of which is therefore not a measure of how far down the explosion has propagated. In this model, it is possible for the hydrothermal explosion to start very near (a few meters) the surface [*Browne and Lawless*, 2001]. The only requirement is a fluid near boiling temperature, and a sudden lowering of pressure (or increase in temperature) leading to the formation of steam.

[35] In the case of the Ashadze or Logatchev venting craters, some characteristics must be taken into account: hydrothermal venting can occur in a classical manner (black smokers) at least during periods of ROV observation and chimneys forming in the craters appear to be episodically destroyed. In addition to mineralogy of deposit the morphology of the crater, the ongoing hydrothermal activity and the breccia deposits identified on the rim of the craters, all this suggest that recurrent hydrothermal eruptions alternate with periods of continuous hydrothermal venting. This may, however, be an oversimplified view. Pressure probe data for the TAG hydrothermal field shows periodic ground deformation that have been interpreted with a geyser-like mechanism [*Sohn et al.*, 2009], yet TAG presents no craters. Tilt cycles with similar periods as those described at TAG by *Sohn et al.* [2009] have been measured at the Logatchev field [*Fabian and Villinger*, 2008]. These authors suggested that pressure fluctuations occur in the hydrothermal upflow zone with a periodicity comparable to those measured near on-land geysers [*Nishimura et al.*, 2006]. The mechanism behind the less common hydrothermal explosions inferred to cause the formation of craters could then be the same mechanism that causes this geyser-like behavior, episodically leading to vapor overpressures in excess of the fracture strength of the host rocks.

[36] Whatever the case, the hydrothermal explosion hypothesis requires a fluid near boiling temperature, and either a drop of pressure, or a rapid increase in temperature, promoting the sudden formation of steam. The drop of pressure may be associated to changes in the permeable pathways

below the vents, or to the release of local overpressures (for example due to gas or fluid trapped below a local impermeable cap [*Fouquet et al.*, 2010]). The nature of the basement probably plays a critical role. *Fouquet et al.* [2010] pointed out that ultramafic-hosted hydrothermal mounds appear to vent through a larger number of individual chimneys than basalt-hosted systems, suggesting that the permeable pathways for hydrothermal fluids are more distributed in the ultramafic basement. The ultramafic material at and very near the seafloor is different from basalts in that it is extensively altered into a friable and highly permeable assemblage of clays, hydroxides and serpentine. In the vicinity of active vents, this material is also locally silicified [*Fouquet et al.*, 2010] and hence quite impermeable. Such heterogeneous material properties could provide favorable conditions for frequent changes in the fluid pathways only a few meters below seafloor, leading to local variations in hydrostatic pressure. Applied to fluids very near boiling, these conditions could promote geyser-like behavior.

[37] At a depth of 4100 m and with a temperature of 355°C the end-member fluids that vent at Ashadze 1 [*Charlou et al.*, 2010] are well below the nominal boiling temperature of a seawater-type fluid. Triggering a hydrothermal explosion under these conditions would therefore require a large pressure release, at least with present-day fluids.

[38] Phase separation processes will produce large volumes of gases in the hydrothermal system [*Foustoukos and Seyfried*, 2007] and these gases, once released, would add to the overpressure of vapor. These phenomena may enhance the explosion triggering process. The Ashadze 2 smokers vent low-salinity fluids that are interpreted as the vapor-dominated component of a phase-separated hydrothermal system [*Charlou et al.*, 2010]. These fluids also have exceptionally high methane and hydrogen contents (up to 26 mmol/kg [*Charlou et al.*, 2010]), similar to those of the Logatchev fluids. Although the role of dissolved gases on the boiling parameters of black smoker fluids is not sufficiently well known to carry the discussion further, such high gas concentrations may play a significant role for crater formation (and possibly also for the geyser-like activity [*Fabian and Villinger*, 2008]) at Logatchev and Ashadze 2.

7. Conclusions

[39] Ultramafic-hosted vents are now commonly described along the MAR and the processes leading to their formation is the focus of active research. In this paper we have documented the geological and hydrothermal setting of the Ashadze vents at the regional to local vent scales. At the regional scale we document the setting of these vents with respect to the detachment fault(s) that bring the deeply derived ultramafic basement rocks to the seafloor. At the local scale we document the morphology of the vents and propose that geyser-like hydrothermal explosions may play a role in their formation.

[40] *Regional scale*. The Ashadze vent fields are located on the western axial valley wall of the Mid-Atlantic Ridge in a transitional domain that links extensive domains of ultramafic seafloor to the north, and basaltic seafloor to the south. Magnetic data acquired across this transition further suggest that it accommodates a 20-km-westward offset of the most recent volcanic activity south of the vents. Shipboard and ROV bathymetry also indicate that decameter-to kilometer-scaled rockslides shape the axial valley wall slopes in the ultramafic seafloor domain, and that at least one of the vent fields (Ashadze 1) lies on a coherent downslided rock mass. ROV bathymetry allows us to infer the position of the present-day point of emergence of the oceanic detachment fault that exhumes the ultramafic basement of the Ashadze vents. The Ashadze 1 vent field at 4100 m depth is located 600 m to the west of this inferred emergence point; the Ashadze 2 field at 3260 m depth is about 6 km to the west. The Ashadze 1 vents also lie some 450 m to the north of a tectonic lineament interpreted as a NE-trending dominantly strike-slip recent fault. Based on these characteristics, we draw a conceptual sketch (Figure 9), which summarizes our preferred working hypothesis for the regional setting of the Ashadze vents. In this sketch, a single hydrothermal cell feeds both fields and mines heat from melt or mush zones associated with the offset southern volcanic axis.

[41] *Local scale*. The local setting of the vents involves structures related to slope failure. This is clear at Ashadze 1 where the vents are set on a coherent landslide rock mass. At Ashadze 2, the vents are located in a linear depression that may have been formed, or reactivated, due to downslope gravitational forces. The Ashadze 1 vent field has hundreds of active and inactive sulfide chimneys. It also includes a 40-m-wide breadcrust-like with radial fissures that could be equivalent to hydrothermal domes seen on land [*Morgan et al.*, 2009]. The black smokers at Ashadze 2 are located inside a crater 40 m in diameter that is similar in its morphology and in its deposits as the Anne-Louise

hydrothermal crater at the Logatchev field [*Petersen et al.*, 2009]. Comparisons of morphology and nature of deposits also can be made with craters in terrestrial hydrothermal areas such as the Yellowstone lakes. We propose that these craters result from explosions associated with geyser-like venting behavior, which would episodically destroy the sulfide chimneys formed during periods of black smoker activity. New cruises allowing for additional sampling and monitoring of these crater-shaped vent sites are now needed to test and refine this hypothesis.

Acknowledgments

[42] We thank the captain and the crew of the R/V Pourquoi Pas?, the team which operates the ROV Victor, and the shipboard scientists of the SERPENTINE cruise. We also give a special thanks to all the Russian teams that carried out previous cruises on the area. We would like to thank the associate editor Barbara John and the reviewers Lisa Morgan and Georgy Cherkashov for their relevant comments and suggestions on how to improve our original manuscript. IPGP contribution 3339.

References

Allen, D. E., and W. E. Seyfried (2004), Serpentinization and heat generation: Constraints from Lost City and Rainbow hydrothermal systems, *Geochim. Cosmochim. Acta*, *68*(6), 1347–1354, doi:10.1016/j.gca.2003.09.003.

Baines, A. G., M. J. Cheadle, B. E. John, and J. J. Schwartz (2008), The rate of oceanic detachment faulting at Atlantis Bank, SW Indian Ridge, *Earth Planet. Sci. Lett.*, *273*(1–2), 105–114, doi:10.1016/j.epsl.2008.06.013.

Barriga, F. J., et al. (1998), Discovery of the Saldanha hydrothermal field on the famous segment of the MAR (36°30′N), *Eos Trans. AGU*, *79*(45), Fall Meet. Suppl., F67.

Batuyev, B. N., A. G. Krotov, V. F. Markov, G. A. Cherkashev, S. G. Krasnov, and Y. D. Lisitsyn (1994), Massive sulphides deposits discovered and sampled at 14°45N, Mid-Atlantic Ridge, *BRIDGE Newsl.*, *6*, 6–10.

Beltenev, V. Y., I. I. Rozhdestvenskaya, A. V. Nescheretov, G. A. Cherkashev, S. M. Sudarikov, A. B. Rumyantsev, V. F. Markov, A. G. Krotov, and E. A. Zhirnov (2002), New data on hydrothermal activity in the area of 12°57′N, MAR: Initial results of the R/V Professor Logatchev cruise 20, *InterRidge News*, *11*, 38–40.

Beltenev, V. Y., et al. (2003), New discoveries at 12°58′N, 44°52′W, MAR: Professor Logatchev-22 cruise, initial results, *InterRidge News*, *12*, 13–14.

Beltenev, V. Y., A. Shagin, V. F. Markov, I. I. Rozhdestvenskaya, T. Stepanova, G. A. Cherkashev, I. Fedorov, A. B. Rumyantsev, and I. Poroshina (2004), A new hydrothermal field at 16°38.4′N, 46°28.5′W on the Mid-Atlantic Ridge, *InterRidge News*, *13*, 5–6.

Beltenev, V. Y., G. V. Ivanov, A. Shagin, M. Sergeyev, I. I. Rozhdestvenskaya, V. Shilov, I. Debretzova, G. A. Cherkashev, M. Samovarov, and I. Poroshina (2005), New hydrothermal sites at 13°N, Mid-Atlantic-Ridge, *InterRidge News*, *14*, 14–16.

Blackman, D. K., J. R. Cann, B. Janssen, and D. K. Smith (1998), Origin of extensional core complexes: Evidence from the Mid-Atlantic Ridge at Atlantis Fracture Zone, *J. Geophys. Res.*, *103*(B9), 21,315–21,333, doi:10.1029/98JB01756.

Bogdanov, Y. A., A. M. Sagalevitch, E. S. Chernyaev, A. M. Ashadze, E. G. Gurvich, V. N. Lukashin, G. V. Ivanov, and V. N. Peresypkin (1995), A study of the hydrothermal field at 14°45′N on the Mid-Atlantic Ridge using the "MIR" submersibles, *BRIDGE Newsl.*, *9*, 9–13.

Bogdanov, Y. A., N. Bortnikov, and I. Vikentiev (1997), New type of modern mineral-forming system: Black smokers of hydrothermal field at 14°45N, Mid-Atlantic Ridge, *Ore Deposits Geol.*, *39*(1), 68–90.

Bougault, H., P. Appriou, P. Bienvenu, P. Cambon, J. L. Charlou, B. Collette, J. P. Donval, L. Dosso, G. Floch, and Y. Fouquet (1990), Campagne RIDELENTE: Structure de la dorsale atlantique, hétérogénéité du manteau et hydrothermalisme, *Oceanol. Acta*, *10*, 276–292.

Bougault, H., J. L. Charlou, Y. Fouquet, H. D. Needham, N. Vaslet, P. Appriou, P. Jean-Baptiste, P. A. Rona, L. Dmitriev, and S. Silantiev (1993), Fast and slow spreading ridges: Structure and hydrothermal activity, ultramafic topographic highs, and CH_4 output, *J. Geophys. Res.*, *98*(B6), 9643–9651, doi:10.1029/93JB00508.

Browne, P. R. L., and J. V. Lawless (2001), Characteristics of hydrothermal eruptions, with examples from New Zealand and elsewhere, *Earth Sci. Rev.*, *52*, 299–331, doi:10.1016/S0012-8252(00)00030-1.

Cann, J. R., D. K. Blackman, D. K. Smith, E. McAllister, B. Janssen, S. Mello, E. Avgerinos, A. R. Pascoe, and J. Escartín (1997), Corrugated slip surfaces formed at ridge–transform intersections on the Mid-Atlantic Ridge, *Nature*, *385*, 329–332, doi:10.1038/385329a0.

Cannat, M. (1993), Emplacement of mantle rocks in the seafloor at mid-ocean ridges, *J. Geophys. Res.*, *98*, 4163–4172, doi:10.1029/92JB02221.

Cannat, M., et al. (1995), Thin crust, ultramafic exposures, and rugged faulting patterns at Mid-Atlantic Ridge (22°N), *Geology*, *23*(1), 49–52, doi:10.1130/0091-7613(1995)023<0049:TCUEAR>2.3.CO;2.

Cannat, M., Y. Lagabrielle, H. Bougault, J. Casey, N. De Coutures, L. Dmitriev, and Y. Fouquet (1997), Ultramafic and gabbroic exposures at the Mid-Atlantic Ridge: Geological mapping in the 15°N region, *Tectonophysics*, *279*, 193–213, doi:10.1016/S0040-1951(97)00113-3.

Cannat, M., H. Ondréas, Y. Fouquet, S. Silantiev, E. Hoise, and F. Fontaine (2007), Geological context of ultramafic-hosted hydrothermal vent fields in the 13–15°N region of the Mid-Atlantic Ridge: Preliminary results of the Serpentine cruise (March 2007), *Eos Trans. AGU*, *88*(52), Fall Meet. Suppl., Abstract T51F-02.

Charlou, J. L., L. Dmitriev, H. Bougault, and H. D. Needham (1988), Hydrothermal CH_4 between 12°N and 15°N over the Mid-Atlantic Ridge, *Deep Sea Res.*, *35*(1), 121–131, doi:10.1016/0198-0149(88)90061-1.

Charlou, J. L., H. Bougault, P. Appriou, T. Nelsen, and P. Rona (1991), Different TDM/CH4 hydrothermal plume signatures: TAG site at 26°N and serpentinized ultrabasic diapir at 15°05′N on the Mid-Atlantic Ridge, *Geochim. Cosmochim. Acta*, *55*(11), 3209–3222, doi:10.1016/0016-7037(91)90484-M.

Charlou, J. L., Y. Fouquet, H. Bougault, J. P. Donval, J. Etoubleau, B. P. Jean, A. Dapoigny, P. Appriou, and P. A. Rona (1998), Intense CH_4 plumes generated by serpentinization of ultramafic rocks at the intersection of the 15°20′N fracture zone and the Mid-Atlantic Ridge, *Geochim. Cosmochim. Acta*, *62*(13), 2323–2333, doi:10.1016/S0016-7037(98)00138-0.

Charlou, J. L., J. P. Donval, Y. Fouquet, P. Jean-Baptiste, and N. Holm (2002), Geochemistry of high H_2 and CH_4 vent fluids issuing from ultramafic rocks at the Rainbow hydrothermal field (36°14′N, MAR), *Chem. Geol.*, *191*(4), 345–359, doi:10.1016/S0009-2541(02)00134-1.

Charlou, J. L., J. P. Donval, C. Konn, H. Ondréas, Y. Fouquet, J. B. Philippe, and E. Fourré (2010), High production and fluxes of H_2 and CH_4 and evidence of abiotic hydrocarbon synthesis by serpentinization in ultramafic-hosted hydrothermal systems on the Mid-Atlantic Ridge, in *Diversity of Hydrothermal Systems on Slow Spreading Ocean Ridges*, *Geophys. Monogr. Ser.*, vol. 188, edited by P. A. Rona et al., pp. 265–296, AGU, Washington, D. C., doi:10.1029/2008GM000752.

Cherkashov, G., V. Beltenev, V. Ivanov, L. Lazareva, M. Samovarov, V. Shilov, T. Stepanova, G. P. Glasby, and V. Kuznetsov (2008), Two new hydrothermal fields at the Mid-Atlantic Ridge, *Mar. Georesour. Geotechnol.*, *26*(4), 308–316, doi:10.1080/10641190802400708.

Cherkashov, G., et al. (2010), Seafloor massive sulfides from the Equatorial Mid-Atlantic Ridge: New discoveries and perspectives, *Mar. Georesour. Geotechnol.*, *28*(3), 222–239, doi:10.1080/1064119X.2010.483308.

deMartin, B. J., R. A. Sohn, J. P. Canales, and S. E. Humphris (2007), Kinematics and geometry of active detachment faulting beneath the Trans-Atlantic Geotraverse (TAG) hydrothermal field on the Mid-Atlantic Ridge, *Geology*, *35*, 711–714, doi:10.1130/G23718A.1.

Dias, Á. S., and F. J. Barriga (2006), Mineralogy and geochemistry of hydrothermal sediments from the serpentinite-hosted Saldanha hydrothermal field (36°34′N; 33°26′W) at MAR, *Mar. Geol.*, *225*(1–4), 157–175, doi:10.1016/j.margeo.2005.07.013.

Dias, Á. S., G. L. Früh-Green, S. M. Bernasconi, F. J. Barriga, and the Seahma Cruise Team (2011), Geochemistry and stable isotope constraints on high-temperature activity from sediment cores of the Saldanha hydrothermal field, *Mar. Geol.*, *279*(1–4), 128–140, doi:10.1016/j.margeo.2010.10.017.

Dick, H. J. B., M. A. Tivey, and B. E. Tucholke (2008), Plutonic foundation of a slow-spreading ridge segment: Oceanic core complex at Kane Megamullion, 23°30′N, 45°20′W, *Geochem. Geophys. Geosyst.*, *9*, Q05014, doi:10.1029/2007GC001645.

Douville, E., J. L. Charlou, E. H. Oelkers, P. Bienvenu, C. F. Jove Colon, J. P. Donval, Y. Fouquet, D. Prieur, and P. Appriou (2002), The Rainbow vent fluids (36°14′N, MAR): The influence of ultramafic rocks and phase separation on trace metal content in Mid-Atlantic Ridge hydrothermal fluids, *Chem. Geol.*, *184*, 37–48, doi:10.1016/S0009-2541(01)00351-5.

Escartín, J., C. Mevel, C. J. MacLeod, and A. M. McCaig (2003), Constraints on deformation conditions and the origin of oceanic detachments: The Mid-Atlantic Ridge core complex at 15°45N, *Geochem. Geophys. Geosyst.*, *4*(8), 1067, doi:10.1029/2002GC000472.

Escartín, J., D. K. Smith, J. Cann, H. Schouten, C. H. Langmuir, and S. Escrig (2008), Central role of detachment faults in accretion of slow-spreading oceanic lithosphere, *Nature*, *455*, 790–794, doi:10.1038/nature07333.

Fabian, M., and H. Villinger (2008), Long-term tilt and acceleration data from the Logatchev Hydrothermal Vent Field, Mid-Atlantic Ridge, measured by the Bremen Ocean Bottom Tiltmeter, *Geochem. Geophys. Geosyst.*, *9*, Q07016, doi:10.1029/2007GC001917.

Fouquet, Y., et al. (1997), Discovery and first submersible investigations on the Rainbow hydrothermal field on the MAR (36°14N), *Eos Trans. AGU*, *78*(46), Fall Meet. Suppl., F832.

Fouquet, Y., et al. (2008), Serpentine cruise–ultramafic hosted hydrothermal deposits on the Mid-Atlantic Ridge: First submersible studies on Ashadze 1 and 2, Logatchev 2 and Krasnov vent fields, *InterRidge News*, *17*, 15–19.

Fouquet, Y., et al. (2010), Geodiversity of hydrothermal processes along the Mid-Atlantic Ridge and ultramafic-hosted mineralization: A new type of oceanic Cu-Zn-Co-Au volcanogenic massive sulfide deposit, in *Diversity of Hydrothermal Systems on Slow Spreading Ocean Ridges*, *Geophys. Monogr. Ser.*, vol. 188, edited by P. A. Rona et al., pp. 321–367, AGU, Washington, D. C., doi:10.1029/2008GM000746.

Foustoukos, D. I., and W. E. Seyfried (2007), Fluid phase separation processes in submarine hydrothermal systems, *Rev. Mineral. Geochem.*, *65*(1), 213–239, doi:10.2138/rmg.2007.65.7.

Fujiwara, T., J. Lin, T. Matsumoto, P. B. Kelemen, B. E. Tucholke, and J. F. Casey (2003), Crustal evolution of the Mid-Atlantic Ridge near the Fifteen-Twenty Fracture Zone in the last 5 Ma, *Geochem. Geophys. Geosyst.*, *4*(3), 1024, doi:10.1029/2002GC000364.

Gebruk, A. V., L. I. Moskalev, P. Chevaldonné, S. M. Sudarikov, and E. S. Chernyaev (1997), Hydrothermal vent fauna of the Logatchev area (14°45′N, MAR): Preliminary results from the first MIR and Nautile dives in 1995, *InterRidge News*, *6*, 10–14.

German, C. R., and J. Lin (2004), The thermal structure of the oceanic crust, ridge-spreading and hydrothermal circulation: How well do we understand their inter-connections?, in *Mid-Ocean Ridges: Hydrothermal Interactions Between the Lithosphere and Oceans*, *Geophys. Monogr. Ser.*, vol. 148, edited by C. R. German, J. Lin, and L. M. Parson, pp. 1–18, AGU, Washington, D. C., doi:10.1029/148GM01.

German, C. R., G. P. Klinkhammer, and M. D. Rudnicki (1996), The Rainbow hydrothermal plume, 36°15′N, MAR, *Geophys. Res. Lett.*, *23*(21), 2979–2982, doi:10.1029/96GL02883.

Grimes, C. B., B. E. John, M. J. Cheadle, and J. L. Wooden (2008), Protracted construction of gabbroic crust at a slow spreading ridge: Constraints from $^{206}Pb/^{238}U$ zircon ages from Atlantis Massif and IODP Hole U1309D (30°N, MAR), *Geochem. Geophys. Geosyst.*, *9*, Q08012, doi:10.1029/2008GC002063.

Janecky, D. R., and W. E. Seyfried (1986), Hydrothermal serpentinization of peridotite within the oceanic crust: Experimental investigations of mineralogy and major element chemistry, *Geochim. Cosmochim. Acta*, *50*(7), 1357–1378, doi:10.1016/0016-7037(86)90311-X.

Johnson, S. Y., W. J. Stephenson, L. A. Morgan, W. C. Shanks III, and K. L. Pierce (2003), Hydrothermal and tectonic activity in northern Yellowstone Lake, Wyoming, *Geol. Soc. Am. Bull.*, *115*(8), 954–971, doi:10.1130/B25111.1.

Karson, J. A., and H. J. B. Dick (1983), Tectonics of ridge-transform intersections at the KANE Fracture-Zone, *Mar. Geophys. Res.*, *6*(1), 51–98, doi:10.1007/BF00300398.

Karson, J. A., G. L. Früh-Green, D. S. Kelley, E. A. Williams, D. R. Yoerger, and M. Jakuba (2006), Detachment shear zone of the Atlantis Massif core complex, Mid-Atlantic

Ridge, 30°N, *Geochem. Geophys. Geosyst.*, *7*, Q06016, doi:10.1029/2005GC001109.

Kelley, D. S., et al. (2001), An off-axis hydrothermal vent field near the Mid-Atlantic Ridge at 30°N, *Nature*, *412*, 145–149, doi:10.1038/35084000.

Krasnov, S. G., et al. (1995), Detailed geological studies of hydrothermal fields in the North Atlantic, in *Hydrothermal Vents and Processes*, edited by L. M. Parson, C. L. Walker, and D. R. Dixon, *Geol. Soc. Spec. Publ.*, *87*, 43–64.

Lowell, R. P., and P. A. Rona (2002), Seafloor hydrothermal systems driven by the serpentinization of peridotite, *Geophys. Res. Lett.*, *29*(11), 1531, doi:10.1029/2001GL014411.

MacLeod, C. J., et al. (2002), Direct geological evidence for oceanic detachment faulting: The Mid-Atlantic Ridge, 15°45N, *Geology*, *30*, 879–882, doi:10.1130/0091-7613(2002)030<0879:DGEFOD>2.0.CO;2.

MacLeod, C. J., R. C. Searle, B. J. Murton, J. F. Casey, C. Mallows, S. C. Unsworth, K. L. Achenbach, and M. Harris (2009), Life cycle of oceanic core complexes, *Earth Planet. Sci. Lett.*, *287*, 333–344, doi:10.1016/j.epsl.2009.08.016.

MacLeod, C. J., J. Carlut, J. Escartín, H. Horen, and A. Morris (2011), Quantitative constraint on footwall rotations at the 15°45′N oceanic core complex, Mid-Atlantic Ridge: Implications for oceanic detachment fault processes, *Geochem. Geophys. Geosyst.*, *12*, Q0AG03, doi:10.1029/2011GC003503.

McCaig, A. M., R. A. Cliff, J. Escartín, A. Fallick, and C. J. MacLeod (2007), Oceanic detachment faults focus very large volumes of black smoker fluids, *Geology*, *35*, 935–938, doi:10.1130/G23657A.1.

McCaig, A. M., A. Delacour, A. E. Fallick, T. Castelain, and G. L. Früh-Green (2011), Detachment fault control on hydrothermal circulation systems: Interpreting the subsurface beneath the TAG hydrothermal field using the isotopic and geological evolution of oceanic core complexes in the Atlantic, in *Diversity of Hydrothermal Systems on Slow Spreading Ocean Ridges*, *Geophys. Monogr. Ser.*, vol. 188, edited by P. A. Rona et al., pp. 207–239, AGU, Washington, D. C., doi:10.1029/2008GM000729.

McKibbin, R., and A. Absar (1989), A model for oxygen isotope transport in hydrothermal systems, *J. Geophys. Res.*, *94*(B6), 7065–7070, doi:10.1029/JB094iB06p07065.

Melchert, B., et al. (2008), First evidence for high-temperature off-axis venting of deep crustal/mantle heat: The Nibelungen hydrothermal field, southern Mid-Atlantic Ridge, *Earth Planet. Sci. Lett.*, *275*, 61–69, doi:10.1016/j.epsl.2008.08.010.

Mendel, V., M. Munschy, and D. Sauter (2005), MODMAG, a MATLAB program to model marine magnetic anomalies, *Comp. Geosci.*, *31*(5), 589–597.

Morgan, L. A., W. P. Shanks, and K. L. Pierce (2002), Possible earthquake-generated wave deposits near Yellowstone Lake: Clues into triggering mechanisms of a large hydrothermal explosion crater, *Eos Trans. AGU*, *83*(47), Fall Meet. Suppl., Abstract V61B-1372.

Morgan, L. A., et al. (2003), Exploration and discovery in Yellowstone Lake: Results from high-resolution sonar imaging, seismic reflection profiling, and submersible studies, *J. Volcanol. Geotherm. Res.*, *122*, 221–242, doi:10.1016/S0377-0273(02)00503-6.

Morgan, L. A., W. P. Shanks, and K. L. Pierce (2006), Super eruption environments make for "super" hydrothermal explosions: Extreme hydrothermal explosions in Yellowstone National Park, *Eos Trans. AGU*, *87*(52), Fall Meet. Suppl., Abstract V33C-0689.

Morgan, L. A., W. C. Pat Shanks III, and K. L. Pierce (2009), Hydrothermal processes above a large magma chamber: Large hydrothermal systems and hydrothermal explosions in Yellowstone National Park, *Spec. Pap. Geol. Soc. Am.*, *459*, 1–95.

Muffler, L. J. P., D. E. White, and A. H. Truesdell (1971), Hydrothermal explosion craters in Yellowstone National Park, *Geol. Soc. Am. Bull.*, *82*, 723–740, doi:10.1130/0016-7606(1971)82[723:HECIYN]2.0.CO;2.

Nishimura, T., M. Ichihara, and S. Ueki (2006), Investigation of the Onikobe geyser, NE Japan, by observing the ground tilt and flow parameters, *Earth Planets Space*, *58*(12), 21–24.

Ondréas, H., M. Cannat, Y. Fouquet, A. Normand, P. M. Sarradin, and J. Sarrazin (2009), Recent volcanic events and the distribution of hydrothermal venting at the Lucky Strike hydrothermal field, Mid-Atlantic Ridge, *Geochem. Geophys. Geosyst.*, *10*, Q02006, doi:10.1029/2008GC002171.

Petersen, S., K. Kuhn, T. Kuhn, N. Augustin, R. Hekinian, L. Franz, and C. Borowski (2009), The geological setting of the ultramafic-hosted Logatchev hydrothermal field (14°45′N, Mid-Atlantic Ridge) and its influence on massive sulfide formation, *Lithos*, *112*(1–2), 40–56, doi:10.1016/j.lithos.2009.02.008.

Picazo, S., M. Cannat, A. Delacour, J. Escartín, S. Rouméjon, and S. Silantyev (2012), Deformation associated with the denudation of mantle-derived rocks at the Mid-Atlantic Ridge 13°–15°N: The role of magmatic injections and hydrothermal alteration, *Geochem. Geophys. Geosyst.*, *13*, Q04G09, doi:10.1029/2012GC004121.

Rona, P. A., L. Widenfalk, and K. Boström (1987), Serpentinized ultramafics and hydrothermal activity at the Mid-Atlantic Ridge Crest near 15°N, *J. Geophys. Res.*, *92*(B2), 1417–1427, doi:10.1029/JB092iB02p01417.

Rona, P. A., H. Bougault, J. L. Charlou, P. Appriou, T. A. Nelsen, J. H. Trefry, G. L. Eberhart, A. Barone, and H. D. Needham (1992), Hydrothermal circulation, serpentinization, and degassing at a rift valley-fracture zone intersection: Mid-Atlantic Ridge near 15°N, 45°W, *Geology*, *20*, 783–786, doi:10.1130/0091-7613(1992)020<0783:HCSADA>2.3.CO;2.

Searle, R. C., M. Cannat, K. Fujioka, C. Mevel, H. Fujimoto, A. Bralee, and L. Parson (2003), FUJI Dome: A large detachment fault near 64°E on the very slow-spreading southwest Indian Ridge, *Geochem. Geophys. Geosyst.*, *4*(8), 9105, doi:10.1029/2003GC000519.

Seyfried, W. E., and W. E. Dibble (1980), Seawater-peridotite interaction at 300°C and 500 bars: Implications for the origin of oceanics serpentites, *Geochim. Cosmochim. Acta*, *44*(2), 309–321, doi:10.1016/0016-7037(80)90139-8.

Seyfried, W. E., Jr., D. I. Foustoukos, and Q. Fu (2007), Redox evolution and mass transfer during serpentinization: An experimental and theoretical study at 200°C, 500 bar with implications for ultramafic-hosted hydrothermal systems at mid-ocean ridges, *Geochim. Cosmochim. Acta*, *71*(15), 3872–3886, doi:10.1016/j.gca.2007.05.015.

Siméoni, P., J. Sarrazin, H. Nouzé, P. M. Sarradin, H. Ondréas, C. Scalabrin, and J. M. Sinquin (2007), Victor 6000: New high resolution tools for deep sea research, "Module de Mesures en Route", *OCEANS07 IEEE Aberdeen Conf. Proc.*, *1–3*, 133–138.

Smith, D. K., J. R. Cann, and J. Escartín (2006), Widespread active detachment faulting and core complex formation near 13°N on the Mid-Atlantic Ridge, *Nature*, *442*, 440–443, doi:10.1038/nature04950.

Smith, D. K., J. Escartín, H. Schouten, and J. R. Cann (2008), Fault rotation and core complex formation: Significant

processes in seafloor formation at slow-spreading mid-ocean ridges (Mid-Atlantic Ridge, 13°–15°N), *Geochem. Geophys. Geosyst.*, *9*, Q03003, doi:10.1029/2007GC001699.

Sohn, R. A., R. E. Thomson, A. B. Rabinovich, and S. F. Mihaly (2009), Bottom pressure signals at the TAG deep-sea hydrothermal field: Evidence for short-period, flow-induced ground deformation, *Geophys. Res. Lett.*, *36*, L19301, doi:10.1029/2009GL040006.

Tivey, M. K., S. E. Humphris, G. Thompson, M. D. Hannington, and P. A. Rona (1995), Deducing patterns of fluid flow and mixing within the TAG active hydrothermal mound using mineralogical and geochemical data, *J. Geophys. Res.*, *100*(B7), 12,527–12,555, doi:10.1029/95JB00610.

Tucholke, B. E., J. Lin, and M. C. Kleinrock (1998), Megamullions and mullion structure defining oceanic metamorphic core complexes on the mid-Atlantic ridge, *J. Geophys. Res.*, *103*(B5), 9857–9866, doi:10.1029/98JB00167.

Wetzel, L. R., and E. L. Shock (2000), Distinguishing ultramafic- from basalt-hosted submarine hydrothermal systems by comparing calculated vent fluid compositions, *J. Geophys. Res.*, *105*(B4), 8319–8340, doi:10.1029/1999JB900382.

Wold, R. J., M. A. Mayhew, and R. B. Smith (1977), Bathymetric and geophysical evidence for an hydrothermal explosion crater in Mary Bay, Yellowstone Lake, Wyoming, *J. Geophys. Res.*, *82*(26), 3733–3738, doi:10.1029/JB082i026p03733.